Almost complete transparency of the $\alpha + {}^{12}$C system at sub-barrier energies

M. Katsuma*

Institut d'Astronomie et d'Astrophysique, Université Libre de Bruxelles, CP226, B-1050 Brussels, Belgium

(Received 4 May 2010; published 17 June 2010)

$\alpha + {}^{12}$C elastic scattering at low energies is analyzed with the optical model. The $\alpha + {}^{12}$C system is transparent over the entire radial range. Weak coupling to other reaction channels seems good enough below $E_{\rm c.m.} = 5$ MeV.

DOI: 10.1103/PhysRevC.81.067603 PACS number(s): 24.10.Ht, 25.55.Ci, 24.30.−v, 26.20.Fj

Low-energy nuclear reactions are generally thought to occur via the complicated internal structure of compound nuclei. In contrast, the direct reaction mechanism, where only a few nucleons (clusters) are activated, is applicable at high energies. Is a very large number of degrees of freedom always involved at low energies? Let us recall, in the present Brief Report, that the key to solve this problem is in the excitation function of elastic scattering.

Elastic event has been extensively studied in the $\alpha + {}^{12}$C system. Elastic scattering above $E_{\rm lab} \approx 100$ MeV is described with the optical model, and interpreted as refractive phenomena [1,2]. ($E_{\rm lab}$ denotes the incident energy in the laboratory system.) The optical model seems to make the reproduction of the data at individual energies for $E_{\rm lab} = 10$–54 MeV, (e.g., Refs. [3,4]). The volume integrals of the deduced optical potential, which are used for the index of the net strength of the potential [5], appear to be similar to those for ^{3}He + ^{12}C and $\alpha + {}^{16}$O elastic scattering [6–8]. The so-called anomalous large angle scattering (ALAS) has been observed in $E_{\rm lab} \approx 10$–35 MeV [3,9–11]. The refractive scattering and ALAS are described by the deep real potential with weak absorption [5,7,12]. These phenomena are considered to indicate that the contribution from the inside of the interaction range plays the significant role in the elastic cross section. The phase shifts have been analyzed below $E_{\rm lab} = 7$ MeV [13,14].

The ^{12}C$(\alpha,\gamma)^{16}$O reaction is an important reaction for astrophysical events [15]. Recently, the low-energy cross sections have been investigated with the direct capture potential model based on the deep potential [16]. The analysis of elastic scattering provides the model with the initial wave, i.e., the $\alpha + {}^{12}$C continuum state including the resonant states.

In the present Brief Report, we analyze the differential cross sections for $\alpha + {}^{12}$C elastic scattering below $E_{\rm c.m.} = 5$ MeV in the center-of-mass system. We show that the contribution from the internal wave [7,12], reflecting on the internal region of the potential, leads to the enhancement of backward scattering. The excitation function is also indicated. The purpose of this report is to illustrate that: (A) The optical model, i.e., the potential model, gives the good description of elastic scattering; (B) The $\alpha + {}^{12}$C system is transparent at sub-barrier energies; (C) Coupling to other channels seems weak.

The optical potential is defined by

$$U(r) = -V(r) - iW(r) + V_c(r), \tag{1}$$

where $V_c(r)$ is the Coulomb potential calculated with a uniform charge sphere of the radius $R_c = 3.5$ fm. The ordinary Woods-Saxon form is used as the functional form of the nuclear potential,

$$f_\xi(r) = \frac{1}{1 + \exp\left[(r - R_\xi)/a_\xi\right]}. \tag{2}$$

The parity-dependent potential is employed as the real part,

$$V(r) = \begin{cases} V_+ f_+(r) & \text{(even)} \\ V_- f_-(r) & \text{(odd)} \end{cases}. \tag{3}$$

V_ξ, R_ξ, and a_ξ are the potential parameters for the even and odd parities. The parameters are set to be $V_+ = 199.7$ MeV, $R_+ = 2.18$ fm, $a_+ = 0.743$ fm, $V_- = 168.1$ MeV, $R_- = 2.76$ fm, and $a_- = 0.567$ fm [16]. Absorption is given by $W(r) = W_I f_I(r)$.

In the analysis at low energies, we encounter the different strength of the potentials reproducing the cross section similarly well. We chose the appropriate strength for the real part of the optical potential. The volume integrals of the potential used here are concordant with those for ^{3}He + ^{12}C and $\alpha + {}^{16}$O elastic scattering [6–8,16]. The derived rotational band of the $\alpha + {}^{12}$C system, shown in Fig. 3 of [16], is similar to that predicted by [17,18].

The differential cross sections for $\alpha + {}^{12}$C elastic scattering are shown in Figs. 1(a) and 1(b). The calculated results are shown by the solid curves. The $W_I = 0$ is used in the calculation. The number near the curve indicates the incident energy in the center-of-mass system. The experimental data are taken from [13,19], and they are converted to Rutherford ratio in the center-of-mass system. To clarify elastic backscattering, we show the angular distributions in Rutherford ratio. The vertical axis is in log scale.

At $E_{\rm c.m.} = 1.100$ MeV, the cross section is dominated by Coulomb scattering, showing approximately constant over the entire angular range, $\sigma/\sigma_R \approx 1$. As the incident energy increases, elastic scattering deviates from pure Coulomb scattering due to the short-range nuclear potential. The interference caused by the nuclear potential results in the enhancement at the backward angles. The absolute values at $\theta_{\rm c.m.} \approx 180^\circ$ are approximately one or two order of magnitude larger than those from pure Coulomb scattering. At $E_{\rm c.m.} = 3.188$ MeV, the contribution from the 4_1^+ resonant state generates the frequent oscillation, compared with the neighboring energies. From the systematic behavior shown in Fig. 1, we consider that

*mkatsuma@gmail.com

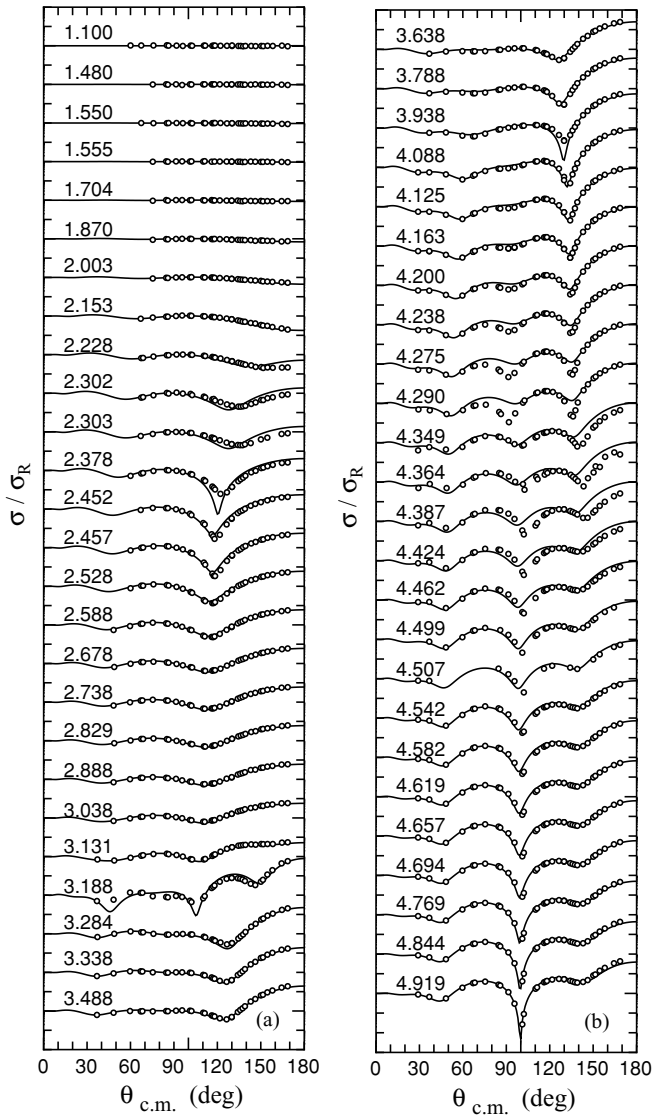

FIG. 1. Differential cross sections of $\alpha + {}^{12}$C elastic scattering at (a) $E_{\text{c.m.}} = 1.100$–3.488 MeV and (b) $E_{\text{c.m.}} = 3.638$–4.919 MeV. The solid curves are the results obtained from the optical model with the parity-dependent potential [16]. The number near the curve indicates the incident energy in the center-of-mass system. The experimental data, converted to Rutherford ratio in the center-of-mass system, are taken from [13,19]. The vertical axis is in log scale.

the characteristic structure in the cross sections appears to be reproduced by the solid curves.

When elastic scattering is interpreted, the scattering amplitude is decomposed into some components associated with the trajectories [5]. The popular techniques are the so-called near-side/far-side decomposition [20] and internal-wave/barrier-wave decomposition [7,12]. The former is used for analyses of the contribution from the edge waves of the interaction range, generally adopted at high energies. The latter is used at low energies. The schematic diagram of the decomposition is illustrated in Fig. 2. The effective barrier, generated by the nuclear + Coulomb + centrifugal potentials, divides the radial distance into the internal and outer regions. The barrier wave corresponds to the scattering wave reflecting on the surface of

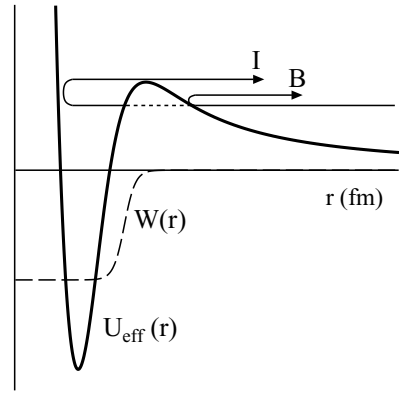

FIG. 2. Schematic diagram of the internal and barrier waves. $U_{\text{eff}}(r)$ is the effective potential, constructed by the nuclear, Coulomb, and centrifugal potentials. "I" and "B" denote the components of the internal wave and barrier wave, respectively. The dashed curve is the tentative absorption $W(r)$ used for the adjustment of the contribution from the internal wave.

the effective barrier. The internal wave reflects on the internal region after penetrating the effective barrier. The technique of the internal/barrier-wave decomposition has been introduced by Brink and Takigawa [12], and developed by Michel and his collaborators, (e.g., Ref. [7]). In the present Brief Report, we roughly estimate how the internal wave interferes with the barrier wave. For the estimation, the tentative absorption $W(r)$, illustrated by the dashed curve in Fig. 2, is introduced. The parameters are set to be $W_I = 10$ MeV and $a_I = 0.2$ fm. The radius parameter is varied in $R_I \leqslant 7$ fm.

The corresponding schematic calculations at $E_{\text{c.m.}} = 2.457$ MeV are shown in Fig. 3. The interference is examined with $R_I = 0.2$, 0.5, 1.0, 3.0, 5.0, and 7.0 fm. "N.A." denotes the result with nonabsorption, which is the same as that in

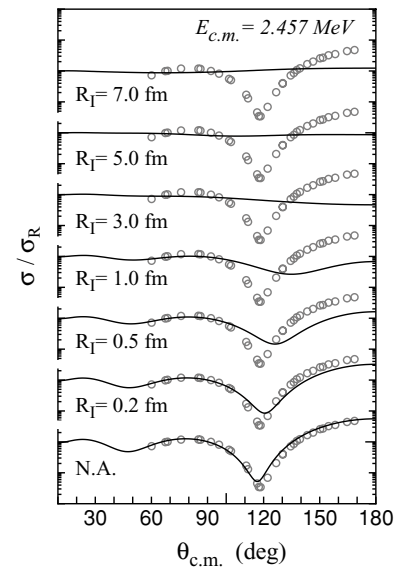

FIG. 3. Interference between the internal and barrier waves at $E_{\text{c.m.}} = 2.457$ MeV. By varying R_I, the contribution from the internal wave is examined. N.A. is the result with nonabsorption, the same as that in Fig. 1. The experimental data are taken from [13,19].

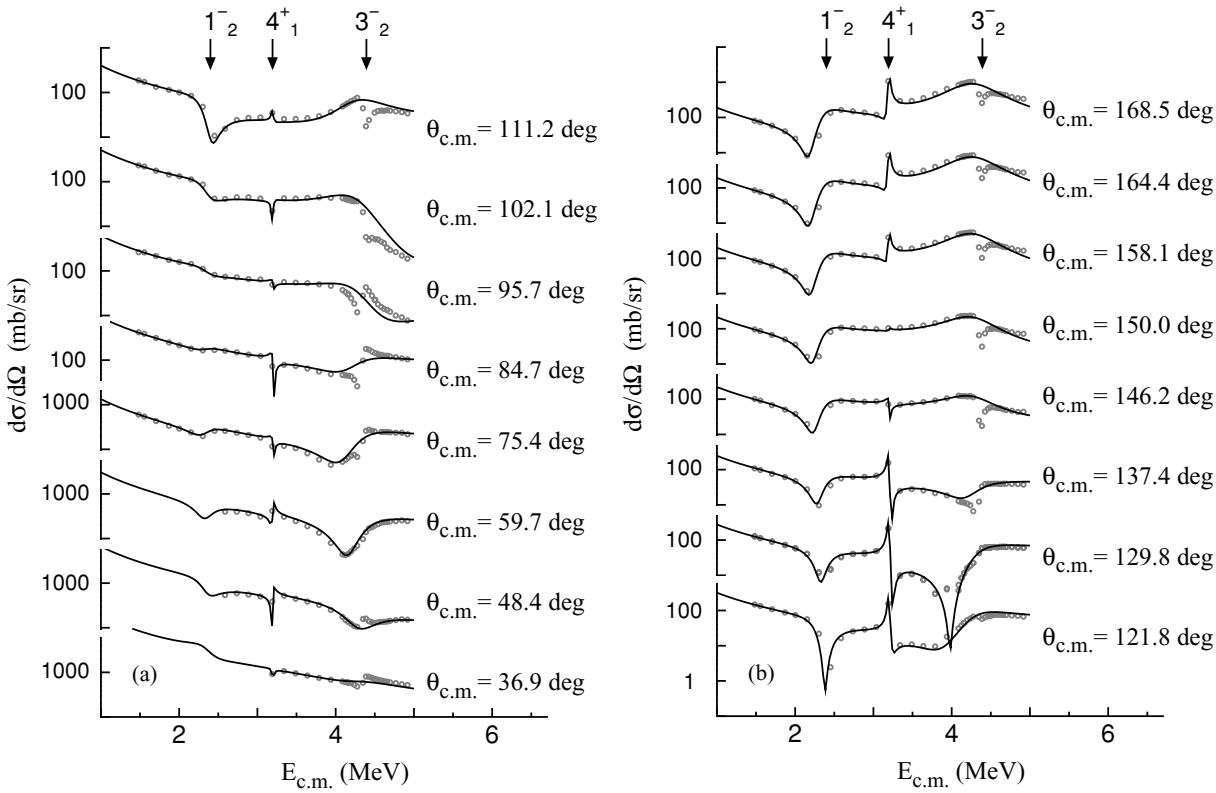

FIG. 4. Excitation functions for $\alpha + {}^{12}$C elastic scattering below $E_{\text{c.m.}} = 5$ MeV. The calculated results are shown by the solid curves. The experimental data are taken from [13,19]. The energy position of the states is indicated by the arrow [21].

Fig. 1. If the internal wave is weakened by the absorption with a large radius $R_I = 7.0$ fm, the differential cross section shows the monotonic decline with increasing scattering angles, becomes approximately $\sigma/\sigma_R \approx 1$ in Rutherford ratio. The large part of the cross section originates from the barrier wave. With decreasing R_I, the internal wave interferes with the barrier wave, and it appears to enhance the cross section at the backward angles. We confirm, from this figure, that the internal wave contribution plays the important role in the backward enhancement.

Let us move back to the lower energies. The contribution from the internal wave becomes weak with decreasing energy, because of the effective barrier [Fig. 1(a)]. Below $E_{\text{c.m.}} =$ 2 MeV, the differential cross sections are not enhanced at the backward angles. At these energies, however, it is quite natural that elastic scattering is dominated by Coulomb scattering. Moreover, the α-particle separation energy of the 0_2^+ ($E_{\text{x}} =$ 6.05 MeV) and 2_1^+ ($E_{\text{x}} = 6.92$ MeV) states in ^{16}O are obtained with the adopted real potential [16]. If elastic scattering were dominated by the strong absorption in $E_{\text{c.m.}} = 0$–2 MeV, the discontinuity of the potential would be unphysical.

The excitation function of $\alpha + {}^{12}$C elastic scattering is illustrated in Fig. 4. The differential cross sections at 16 angles are plotted as a function of the incident energy. As shown in this figure, the excitation function is found to be well described with the model calculation, shape elastic scattering, shown by the solid curves. The resonant behavior originates from the single particle motion of the α particle around ^{12}C. Judging from the reproduction, the contribution from the coupling to other reaction channels would be negligible except the vicinity of the narrow resonances at $E_{\text{c.m.}} \approx 4.3$ MeV. If the coupling to other channels were strong below $E_{\text{c.m.}} = 5$ MeV, the excitation function would have more complicated frequent structure.

The experimental energy position of the 1_2^-, 4_1^+, and 3_2^- resonances [21] is indicated by the arrow in Fig. 4. The excited states in ^{16}O near the α-particle threshold, including the 0_2^+ and 2_1^+ states, are interpreted fairly well by the simple $\alpha + {}^{12}$C configuration, and they construct the rotational bands of which the total quantum numbers correspond to $N = 8$ and $N = 9$ [16]. The existence of this rotational band is known as the so-called Ikeda threshold energy rule (e.g., Ref. [22]).

In the microscopic point of view, the Pauli principle compels the total wave function to be antisymmetric under the interchange of nucleons. Provided the internal wave functions of α-particle and ^{12}C are individually antisymmetrized, the antisymmetrization between nucleons of two nuclei should be taken into account. Some insight into the antisymmetrization, have been provided by the studies with the resonating group method (RGM), lead to the use of the deep real potential (e.g., Ref. [23]). The adopted empirical potential is expected to correspond to the local potential equivalent to the result from microscopic theories. The derived relative wave function between the α particle and ^{12}C is thus considered to have the sufficient node, appropriate local momentum at short distances, and to satisfy the Pauli principle.

The R- and K-matrix methods have been employed to analyze $\alpha + {}^{12}\mathrm{C}$ elastic scattering, ${}^{12}\mathrm{C}(\alpha,\gamma){}^{16}\mathrm{O}$, and β-delayed α spectrum of ${}^{16}\mathrm{N}$ (e.g., Refs. [24,25]). However, the contributions from the 1^-_1 ($E_x = 7.12$ MeV) and 3^-_1 ($E_x = 6.13$ MeV) states below the $\alpha + {}^{12}\mathrm{C}$ threshold may seem to be a source of controversy [16,26,27]. These states do not belong to the $\alpha + {}^{12}\mathrm{C}$ rotational band, and they are considered to be well described by the shell model [16–18,28,29]. Under the influence of the transparency, how could they contribute largely above the particle threshold? At least, in the analyses of ${}^{16}\mathrm{N}(\beta){}^{16}\mathrm{O}^*(\alpha){}^{12}\mathrm{C}$, the excited state ${}^{16}\mathrm{O}^*$ may not seem to be described by the compound nuclear states independent of the synthesis process, because life time is very short, especially the state with a broad width or the background state.

In summary, we have confirmed that the optical model with the parity-dependent potential and non-absorption makes the successful reproduction of the differential cross section for $\alpha + {}^{12}\mathrm{C}$ elastic scattering below $E_{\mathrm{c.m.}} = 5$ MeV. The interference between the internal and barrier waves has been examined by adjusting the tentative absorption. We have illustrated, from the schematic calculation, that the barrier wave component does not show the backward enhancement, and that the internal wave plays the important role in the characteristic angular distribution. The excitation function of elastic scattering appears to be described by only the simple $\alpha + {}^{12}\mathrm{C}$ configuration. We, therefore, consider that weak coupling to other channels is good enough below $E_{\mathrm{c.m.}} = 5$ MeV, judging from the small difference between the calculated result and experimental data.

Not only the transparency of the system but also the single-particle α orbital surviving in the excitation function seems to reinforce the applicability of the potential model with the simple configuration in the analysis of the ${}^{12}\mathrm{C}(\alpha,\gamma){}^{16}\mathrm{O}$ reaction [16].

The author is grateful to Prof. Y. Kondō and Prof. Y. Sakuragi for the discussion about the molecular resonance and nuclear rainbow in the early days of collaboration. He thanks Professors P. Descouvemont, M. Dufour, J.-M. Sparenberg, and A. E. Champagne for calling his attention to the present work. He also thanks M. Arnould, A. Jorissen, K. Takahashi, and H. Utsunomiya for their hospitality and encouragement. This work has been done in part by the Interuniversity Attraction Pole IAP 5/07 of the Belgian Federal Science Policy and by the Konan University – Université Libre de Bruxelles convention.

[1] A. Ingemarsson, A. Auce, and R. Johansson, Phys. Rev. C **49**, 1609 (1994).
[2] D. T. Khoa, Phys. Rev. C **63**, 034007 (2001).
[3] J. B. A. England *et al.*, Nucl. Phys. A **284**, 29 (1977).
[4] H. Abele *et al.*, Z. Phys. A **326**, 373 (1987).
[5] M. E. Brandan and G. R. Satchler, Phys. Rep. **285**, 143 (1997).
[6] H.-J. Trost *et al.*, Nucl. Phys. A **337**, 377 (1980).
[7] F. Michel *et al.*, Phys. Rev. C **28**, 1904 (1983).
[8] F. Michel, G. Reidemeister, and Y. Kondō, Phys. Rev. C **51**, 3290 (1995).
[9] T. Mikumo, J. Phys. Soc. Jpn. **16**, 1066 (1961).
[10] T. Mikumo *et al.*, J. Phys. Soc. Jpn. **15**, 1158 (1960).
[11] H. Oeschler, H. Fuchs, and H. Schröter, Nucl. Phys. A **202**, 513 (1973).
[12] D. M. Brink and N. Takigawa, Nucl. Phys. A **279**, 159 (1977).
[13] R. Plaga *et al.*, Nucl. Phys. A **465**, 291 (1987).
[14] P. Tischhauser *et al.*, Phys. Rev. C **79**, 055803 (2009).
[15] C. E. Rolfs and W. S. Rodney, *Cauldrons in the Cosmos* (The University of Chicago Press, Chicago, 1988).
[16] M. Katsuma, Phys. Rev. C **78**, 034606 (2008).
[17] B. Buck and J. A. Rubio, J. Phys. G **10**, L209 (1984).
[18] B. Buck, C. B. Dover, and J. P. Vary, Phys. Rev. C **11**, 1803 (1975).
[19] International Network of Nuclear Reaction Data Centres, Experimental Nuclear Reaction Data (EXFOR) No. C0064. [http://www.nndc.bnl.gov/exfor/exfor00.htm].
[20] R. C. Fuller, Phys. Rev. C **12**, 1561 (1975).
[21] D. R. Tilley, H. R. Weller, and C. M. Cheves, Nucl. Phys. A **564**, 1 (1993).
[22] K. Ikeda, H. Horiuchi, and S. Saito, Prog. Theor. Phys. Suppl. **68**, 1 (1968).
[23] H. Horiuchi, Prog. Theor. Phys. **69**, 886 (1983).
[24] L. R. Buchmann and C. A. Barnes, Nucl. Phys. A **777**, 254 (2006).
[25] X. D. Tang *et al.*, Phys. Rev. C **81**, 045809 (2010).
[26] M. Katsuma, Phys. Rev. C **81**, 029804 (2010).
[27] P. Descouvemont, M. Dufour, and J. M. Sparenberg, Phys. Rev. C **81**, 029803 (2010).
[28] Y. Suzuki, Prog. Theor. Phys. **55**, 1751 (1976).
[29] Y. Fujiwara *et al.*, Prog. Theor. Phys. Suppl. **68**, 29 (1980).